Regulation of spontaneous rhythmic activity and organization of pacemakers as memory traces by spike-timing-dependent synaptic plasticity in a hippocampal model

Motoharu Yoshida[1,*] and Hatsuo Hayashi[2,†]
[1]*Department of Computer Science and Electronics, Graduate School of Computer Science and Systems Engineering, Kyushu Institute of Technology, Iizuka 820-8502, Japan*
[2]*Department of Brain Science and Engineering, Graduate School of Life Science and Systems Engineering, Kyushu Institute of Technology, Wakamatsu-ku, Kitakyushu 808-0196, Japan*
(Received 9 May 2003; published 29 January 2004)

It is widely believed that memory traces can be stored through synaptic conductance modification of dense excitatory recurrent connections (ERCs) in the hippocampal CA3 region, namely associative memory. ERCs, on the other hand, are crucial to maintain spontaneous rhythmic activity in CA3. Since it is experimentally suggested that synaptic conductances of ERCs are modified through spike-timing-dependent synaptic plasticity (STDP), rhythmic activity might modify ERCs with the presence of STDP because rhythmic activity involves discharges of pyramidal cells. Memory patterns that are stored using ERCs might thus be modified or even destroyed. Rhythmic activity itself might also be modified. In this study, we assumed that the synaptic modification in the hippocampal CA3 was subject to STDP, and examined the coexistence of memory traces and rhythmic activity. The activity of the network was dominated by radially propagating burst activities (radial activities) that initiated at local regions and acted as pacemakers. The frequency of the rhythmic activity converged into one specific frequency with time, depending on the shape of the STDP functions. This indicates that rhythmic activity could be regulated by STDP. By applying theta burst stimulation locally to the network, we found that the stimulation whose frequency was higher than that of the spontaneous rhythmic activity could organize a new radial activity at the stimulus site. Newly organized radial activities were preserved for seconds after the termination of the stimulation. These results imply that CA3 with STDP has an ability to self-regulate rhythmic activity and that memory traces can coexist with the rhythmic activity by means of radial activity.

DOI: 10.1103/PhysRevE.69.011910 PACS number(s): 87.18.Hf, 05.65.+b, 87.18.Bb, 87.18.Sn

I. INTRODUCTION

The hippocampus is a brain tissue essential for storing and recalling memories. Underlying mechanisms for storing memories are widely believed to be modification of synaptic conductances between neurons. The hippocampal CA3 network has dense excitatory recurrent connections (ERCs) between pyramidal cells [1,2] and it is widely believed that CA3 has the capability for storing information by synaptic potentiation between specific neurons: so called associative memory [3–5].

Recently, much work has been done about hippocampal activity related to spatial animal behavior. Place cells, which fire corresponding primarily to an animal's position, have been found in the CA3 region as well as other regions in the hippocampus [6,7]. Nakazawa and his colleagues compared knockout (KO) mice that had no NMDA receptor in the CA3 region with wild type mice, in spatial tasks [8]. The KO mice could not modify synaptic conductances between ERCs in CA3 because of the absence of NMDA receptors. The KO and wild type mice could perform equally well the spatial task using spatial cues as landmarks. However, the spatial abilities of KO and wild type mice were different when some of the spatial cues were missing. The spatial ability of the KO mice was significantly worse compared to the wild type. This suggests that information about spatial cues was linked together in wild type mice, producing an associative memory through modification of synaptic conductances of ERCs in CA3. Because of the associative memory, wild type mice would have been able to reproduce activity of CA3 that was the same or similar to the activity produced under full cue condition, even if some cues were missing.

The hippocampal CA3 region shows rhythmic activity such as theta rhythm. Whether the CA3 region generates theta rhythm by itself or only receives theta rhythm from other regions of the brain has been a matter of controversy. However, many experimental results support the idea that CA3 is a theta rhythm generator [9]. CA3 pyramidal cells have intrinsic properties to oscillate in a theta frequency range [10]. The CA1 stratum radiatum and dentate molecular layer are axonal target regions of CA3 pyramidal cells. Theta rhythms observed in those regions are strongly correlated to each other, while these rhythms are weakly correlated to theta rhythms that are projected from the entorhinal cortex [11]. Wu and his colleagues have observed the rhythmic activity of CA3 in an isolated hippocampus [12]. They have also reported that the rhythmic activity almost disappears when AMPA-receptor mediated channels are blocked. These findings imply that the CA3 network can generate rhythmic activity spontaneously and ERCs are crucial for rhythm generation.

Long-term synaptic modification that depends on the relative timing of pre- and postsynaptic spikes has been observed experimentally in many brain tissues including the hippoc-

*Email address: a792013m@iizuka.isc.kyutech.ac.jp
†Author to whom correspondence should be addressed. Email address: hayashi@brain.kyutech.ac.jp

ampal CA3 region [13–17]; this is known as spike-timing-dependent synaptic plasticity (STDP). As one pair of pre- and postsynaptic spikes can modify the synaptic conductance under the consequence of STDP, synaptic modifications such as long-term potentiation (LTP) and long-term depression (LTD) do not require strong activation of neurons or high frequency stimulation from outside of the network. This implies that synaptic modification might occur continuously in neural networks that cause spontaneous activity. Therefore, spontaneous rhythmic activity in the CA3 network might modulate the strength of ERCs and might change its own rhythmic activity due to ERC modification. This further implies that even if any kinds of memory traces, such as associative memory, are stored as spatially distributed conductances of ERCs, they might be altered or destroyed by the spontaneous rhythmic activity.

In this study, using a hippocampal CA3 network model that causes spontaneous rhythmic activity, we investigated (1) how the temporal and spatial features of spontaneous rhythmic activity were altered by STDP, and (2) how input signals from outside of the network could organize memory traces that could coexist with the rhythmic activity. As a result of numerical simulations, we found that radially propagating activities which initiated at local regions and acted as pacemakers emerged in the CA3 network. When radially propagating activities were organized, the frequency of the spontaneous rhythmic activity converged into a specific frequency, depending on the shape of the STDP function. We also found that burst stimulation, whose frequency was higher than that of the spontaneous rhythmic activity, could organize a new radially propagating activity at the stimulus site, while lower frequency burst stimulation could not. Newly organized radially propagating activities were preserved for several seconds after the termination of the stimulation. These results imply that the hippocampal CA3 region has the ability to regulate its own rhythmic activity and preserved radially propagating activities can coexist with rhythmic activity as memory traces.

II. METHODS

A. The hippocampal CA3 network model

1. Cell models

The pyramidal cell model is a single-compartment model developed by Tateno *et al.* [18]. The equations of the pyramidal cell model are as follows:

$$\begin{aligned} C dV/dt = {} & g_{\mathrm{Na}} m^2 h (V_{\mathrm{Na}} - V) + g_{\mathrm{Ca}} s^2 r (V_{\mathrm{Ca}} - V) \\ & + g_{\mathrm{Ca(low)}} s_{\mathrm{low}}^2 r_{\mathrm{low}} (V_{\mathrm{Ca}} - V) + g_{\mathrm{K(DR)}} n (V_{\mathrm{K}} - V) \\ & + g_{\mathrm{K(A)}} a b (V_{\mathrm{K}} - V) + g_{\mathrm{K(AHP)}} q (V_{\mathrm{K}} - V) \\ & + g_{\mathrm{K(C)}} c \min(1, \chi/250) (V_{\mathrm{K}} - V) + g_{\mathrm{L}} (V_{\mathrm{L}} - V) \\ & + g_{\mathrm{af}} (V_{\mathrm{syn(e)}} - V) + I_{\mathrm{syn}}, \end{aligned} \tag{1}$$

$$dz/dt = \alpha_z (1 - z) - \beta_z z, \tag{2}$$

$$d\chi/dt = -\phi I_{\mathrm{Ca}} - \beta_\chi \chi. \tag{3}$$

The constants g_{y} and V_{y} are the maximum conductance and the equilibrium potential for ion channels, respectively; the subscript y stands for Na, Ca, Ca(low), K(DR), K(A), K(AHP) and K(C). The constants, g_{L} and g_{af}, are the conductances for leakage and afferent excitatory synapses, and V_{L} and $V_{\mathrm{syn(e)}}$ are the equilibrium potential of the leakage and the excitatory synapses, respectively. Different g_{af} values ($g_{\mathrm{af\ center}}$, $g_{\mathrm{af\ edge}}$ and $g_{\mathrm{af\ corner}}$) were used depending on the location of the pyramidal cells in the network, as stated in the following section. The variable z is the ion-gating variable; z stands for m, h, s, r, s_{low}, r_{low}, n, a, b, q and c. I_{Ca} is the sum of the second and the third terms on the right-hand side of Eq. (1). I_{syn} is the sum of synaptic currents. Parameter values and equations of the rate constants, α_z and β_z, are listed in Appendix A.

The low threshold Ca^{2+} channel [the third term on the right-hand side of Eq. (1)] provides persistent inward Ca^{2+} current as observed in the real CA3 pyramidal cell [19]. Because of this inward current, the CA3 pyramidal cell does not have a resting potential. The membrane potential is depolarized slowly and the cell fires spontaneously without any external stimulation (even if the value of g_{af} is 0 μS). Firing involves further Ca^{2+} influx mainly through the high threshold Ca^{2+} channel [the second term on the right-hand side of Eq. (1)] and intracellular Ca^{2+} concentration [χ in Eq. (1)] increases during repetitive firing. The increase in the Ca^{2+} concentration in turn activates the Ca^{2+}-activated K^+ and the AHP K^+ currents [the sixth and seventh terms on the right-hand side of Eq. (1)] and the K^+ currents hyperpolarize the membrane potential. This hyperpolarization interrupts spikes, and burst is formed [upper trace in Fig. 1(b)].

In this way, the Ca^{2+} and Ca^{2+}-activated K^+ currents cause slow oscillations, and the Na^+ and delayed K^+ currents cause fast oscillations (spikes). Because of the interaction of the fast and slow oscillations, the pyramidal cell model shows successive bifurcations, from periodic bursts to periodic single spike trains through chaos, with increase in the constant outward current. These firing patterns agree well with the experimental observations [18].

Interneurons in the hippocampus can be classified into fast spiking and nonfast spiking neurons [20]. As the fast spiking neurons do not cause adaptation, the fast spiking neurons would have greater influence on the activity of neural networks. We therefore adopted fast spiking interneurons in this study. Although the fast spiking interneurons have Ca^{2+}-activated K^+ channels, it is supposed that elevation of the intracellular Ca^{2+} concentration is suppressed by an intracellular Ca^{2+} buffer, and effects of the Ca^{2+}-activated K^+ channels are small [21]. The interneuron model therefore contains only Na^+, delayed K^+, and leak currents. The parameters of the interneuron model were adjusted to reproduce the firing pattern of the interneuron observed experimentally by Kawaguchi and Hama [20], and Miles [22]. The equations of the interneuron model are as follows:

$$\begin{aligned} C dV/dt = {} & g_{\mathrm{Na}} m^3 h (V_{\mathrm{Na}} - V) + g_{\mathrm{K(DR)}} n^4 (V_{\mathrm{K}} - V) \\ & + g_{\mathrm{L}} (V_{\mathrm{L}} - V) + I_{\mathrm{syn}}, \end{aligned} \tag{4}$$

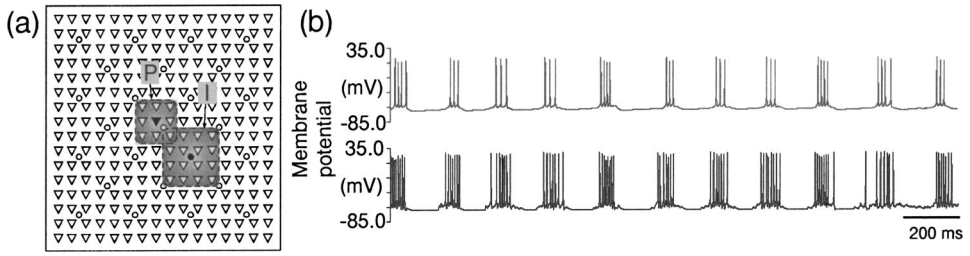

FIG. 1. Hippocampal CA3 network model and firing patterns of neurons. (a) CA3 network model. 256 pyramidal cells (triangles) are placed on 16×16 lattice points. Each pyramidal cell is connected to the nearest and the next-nearest neighbors through excitatory synapses. For example, the pyramidal cell shown by the filled triangle is connected to/from pyramidal cells within the area P. 25 interneurons (circles) are placed uniformly among pyramidal cells. Each interneuron receives excitatory synaptic input from 16 nearby pyramidal cells and inhibits the same cells. For example, the interneuron shown by the filled circle is connected from/to pyramidal cells within the area I. (b) Firing patterns. The upper trace is the firing pattern of the pyramidal cell shown by the filled triangle in (a). The lower trace is the firing pattern of the interneuron closest to that pyramidal cell. Pyramidal cells cause bursts of firing spontaneously, and interneurons fire because of excitatory synaptic input from nearby pyramidal cells.

$$dz/dt = \alpha_z(1-z) - \beta_z z. \tag{5}$$

The lower trace in Fig. 1(b) shows a firing pattern of an interneuron in the network. See Appendix A for the parameter values and voltage dependence of the rate constants, α_z and β_z.

2. Connectivity in the network

In the CA3 network model, 256 pyramidal cells are placed on 16×16 lattice points [Fig. 1(a)]. Each pyramidal cell is recurrently connected to the nearest and next-nearest neighbors through excitatory synapses (ERCs) (e.g., the area P for the pyramidal cell indicated by the filled triangle). 25 interneurons are placed uniformly among the pyramidal cells. Each interneuron receives excitatory synaptic input from 16 nearby pyramidal cells and inhibits the same cells (e.g., the area I for the interneuron indicated by the filled circle). The equations for each of the synaptic currents take the following form:

$$I_{\mathrm{syn}} = g_{\mathrm{syn}}(V_{\mathrm{syn}} - V), \tag{6}$$

$$g_{\mathrm{syn}} = C_{\mathrm{syn}}(\exp(-t/\tau_{1(\mathrm{syn})}) - \exp(-t/\tau_{2(\mathrm{syn})})). \tag{7}$$

The subscript ''syn'' is referred to as pp, pi, and ip for excitatory recurrent connections between pyramidal cells (ERCs), excitatory connections from pyramidal cells to interneurons, and inhibitory connections from interneurons to pyramidal cells, respectively. Excitatory synaptic input through mossy fiber takes the same form as Eqs. (6) and (7), where ''syn'' is referred to as stim. While synaptic conductances, C_{pi}, C_{ip} and C_{stim}, are fixed throughout this paper and uniform over the whole network, each C_{pp} is modified independently through STDP during simulation (see below). Parameter values in Eqs. (6) and (7) are listed in Appendix B. The delay of the synaptic transmission is 1 ms at all kinds of synapses.

In the present network model, pyramidal cells placed on the edges and next to the edges of the network receive inhibitory input from only one interneuron, while the others receive it from two interneurons. Moreover, pyramidal cells on the edges and the corners receive excitatory input from only five and three nearby pyramidal cells respectively, while others receive it from eight pyramidal cells. Less inhibition and less excitation make pyramidal cells fire with shorter interburst interval because of less hyperpolarization and less Ca^{2+} influx. To reduce these edge effects, g_{af} values of pyramidal cells placed at the corners ($g_{\mathrm{af\ corner}}$) and on the edges ($g_{\mathrm{af\ edge}}$) were set smaller than those of the rest of the network ($g_{\mathrm{af\ center}}$), as listed in Appendix A.

B. Synaptic modification

ERC conductances (C_{pp}) in CA3 can be modified by STDP as experimentally shown [15]. Synaptic conductances from pyramidal cells to interneurons and vice versa in CA3 might also be modified by STDP, but experimental results suggesting such synaptic modification have not yet been reported. In this model, synaptic conductances between pyramidal cells and interneurons are therefore fixed and uniform.

The modification function $F(\Delta t)$ is as follows:

$$F(\Delta t) = \begin{cases} M\exp((\Delta t - T_{\mathrm{bias}})/\tau) & \text{if } -T \leqslant \Delta t - T_{\mathrm{bias}} < 0, \\ -M\exp(-(\Delta t - T_{\mathrm{bias}})/\tau) & \text{if } 0 < \Delta t - T_{\mathrm{bias}} \leqslant T, \\ 0 \quad \text{otherwise.} \end{cases} \tag{8}$$

Δt denotes the relative spike timing between pre- and postsynaptic spikes (the time of the presynaptic spike minus the time of the postsynaptic spike). The time constant τ and the maximal modification M are 20 ms and 0.05, respectively, throughout this paper. The parameter T_{bias} shifts the STDP function to the left or right along the Δt axis. When the value of $T_{\mathrm{bias}}=0$, $F(\Delta t)$ is a well-tested STDP function [23–25], which is a simple approximation of the experimental results obtained by Bi and Poo [16] using dissociated and cultured hippocampal cells. Figure 3(f) shows the shape of $F(\Delta t)$ with $T_{\mathrm{bias}}=0$. The STDP function is symmetric with respect to the origin when T_{bias} is 0. Experimentally observed

STDP function for ERCs in CA3 is asymmetric with respect to the origin [15]. A variety of values of T_{bias} were tested in Sec. III B to investigate effects of the asymmetric shape of the STDP function on rhythm regulation [Figs. $4(a_i)-(a_{iii})$]. By setting $T=100$ ms, we neglected synaptic modification in the Δt range where the absolute amount of the modification function ($|F(\Delta t)|$) was less than 0.00034. The modification of the ERC conductance C_{pp} was limited to the range $C_{min} \leqslant C_{pp} \leqslant C_{max}$, where C_{min} and C_{max} were 0.0015 and 0.005 μS, respectively. Each pair of pre- and postsynaptic spikes modifies C_{pp} by the following equation:

$$C_{pp} \rightarrow C_{pp} + C_{max} F(\Delta t). \tag{9}$$

However, if $C_{pp} > C_{max}$, C_{pp} was set to C_{max}, and if $C_{pp} < C_{min}$, C_{pp} was set to C_{min} to keep the value of C_{pp} in the range between C_{min} and C_{max}.

C. Relative spike timing histogram and estimation of plastic change of C_{pp}

In Secs. III B to D, histograms of relative spike timing Δt will be shown. Every pair of spike timing of pre- and postsynaptic cells during a specific time window [for example, 35–50 s in Fig. 4(b)] was counted to obtain a histogram of the relative spike timing Δt at a synapse. The range of Δt was $-T$ to T, and the bin of Δt was 5 ms. Note that in Sec. III B, histograms at every ERC synapse in the network are added up to obtain a total relative spike timing histogram. In Secs. III C and D, histograms at synapses from proximal to distal cells are added up. The histograms are normalized by the total number of spike pairs.

The value E_{PD} was defined as follows, to estimate whether C_{pp} was potentiated or depressed on average.

$$E_{PD} = \sum_{i=-19}^{20} [H(i) F(5i - 5/2)]. \tag{10}$$

$H(i)$ is the height of the bar at the ith bin of Δt in the relative spike timing histogram at a synapse. $F(5i-5/2)$ is the value of the STDP function at the center of the ith bin. The positive and negative values of E_{PD} indicate that C_{pp} is potentiated and depressed, respectively, on average in the time window.

D. Measurement of spatially asymmetric ERCs and degree of radial ERC

Each pyramidal cell receives ERCs from its neighboring pyramidal cells as mentioned above. These ERC conductances, C_{pp}s, are modified by STDP; some are potentiated and the others are depressed during simulation. This causes spatially asymmetric C_{pp}s. The spatial asymmetry is represented by the orientation and length of the bars located at every location of pyramidal cells in the network, as shown in Fig. 2(a) and Fig. 3(a). The bar for ith pyramidal cell is obtained as follows. Vectors corresponding to excitatory connections are obtained first; each vector is oriented from one of the presynaptic pyramidal cells (one of the neighbors) to the postsynaptic cell (ith cell) and the length of the vector is proportional to C_{pp}. Next, these vectors are summed and the length of the summed vector is normalized by dividing it with $C_{max}(1+\sqrt{2})$ so that the length of the normalized vector $\mathbf{V}_i$ does not exceed unity. The vector $\mathbf{V}_i$ is shown as the bar originating from the position of the ith pyramidal cell. Therefore, activity of the pyramidal cells is most likely to propagate to the direction of the bar. Pyramidal cells that may have bars whose length is unity (maximal) are only at the edge of the network where the cells have less than eight ERCs. In the other area where pyramidal cells have eight ERCs, the maximum length of the bars is 0.7, because even if one of the ERC conductances C_{pp} is 0.005 μS (C_{max}), the ERC conductance on the opposite side is at least 0.0015 μS (C_{min}).

The value D_{rad} was defined as follows to measure the degree of radial ERC (see Sec. III A for radial-ERC):

$$D_{rad} = \frac{\Sigma_i^n (V_i I_i)}{n}. \tag{11}$$

$\mathbf{V}_i$ is the vector corresponding to the bar at the ith pyramidal cell, as mentioned above. $\mathbf{I}_i$ is the vector whose orientation is from the center of the radial ERC (the center of the cluster of cells stimulated; see Sec. III C and D) to the position of the ith pyramidal cell, and whose length is unity. The value D_{rad} is obtained in a circular area whose radius is six times larger than the distance between pyramidal cells, as indicated in Figs. 5(b) and 6(b). n is the number of pyramidal cells that are in the circular area and summation is done among these cells. The value of D_{rad} is the largest when each $\mathbf{V}_i$ in the circle is identical to $\mathbf{I}_i$ and gradually decreases as the difference between $\mathbf{V}_i$ and $\mathbf{I}_i$ increases.

E. Measurement of spatial dynamics

The spatial dynamics of the network was measured as directions of propagation of burst activity at locations of pyramidal cells, and shown as wedge-shaped arrows [Fig. 2(e), Fig. 3(e), and Fig. $6(e_{viii})$]. To identify the directions of propagation of burst activity, we first observed times of burst occurrence. As each burst consisted of several spikes, we used the time of the first spike to define the time of the burst.

The wedge-shaped arrow at each pyramidal cell (the ith pyramidal cell) was obtained as follows. For occurrence of each burst of the ith cell at time bt_i, bt_i was compared to the times of bursts of the nearest eight surrounding pyramidal cells. At each of the eight surrounding cells, the time of the burst occurrence, bt_j, closest in time to bt_i was detected ($j=1$ to 8 for each i). The differences between bt_i and $bt_j (delay_{ij} = bt_j - bt_i)$ were obtained.

Since wave fronts of burst propagation are roughly vertical to the direction of propagation, the ith and the jth cells on the wave front fire at almost the same time ($delay_{ij} \sim 0$). On the other hand, the jth cell that produces the largest $delay_{ij}$ (we define such j as J) corresponds roughly to the direction of propagation from the ith cell. The vector orienting from the ith cell to the Jth cell was obtained; the length of the vector was unity.

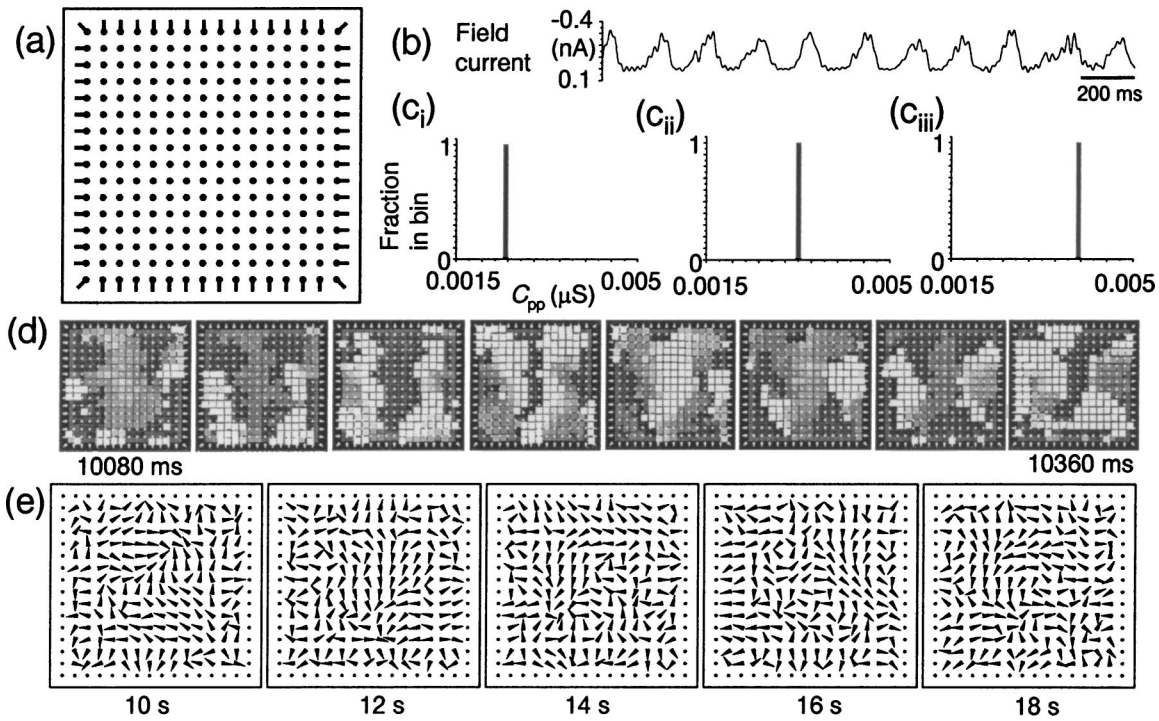

FIG. 2. Spontaneous rhythmic activity before applying STDP algorithm. (a) Spatial pattern of C_{pp}s at 10 s. The size of filled circles placed on 16×16 lattice points indicates the average C_{pp}s from surrounding pyramidal cells to each pyramidal cell. The bar extending from each circle is the vector V_i (see Methods), which indicates the spatial asymmetry of C_{pp}s. (b) Field current obtained from synaptic currents at the center of the network. (c_i)–(c_{iii}) Distributions of C_{pp} in the network at 10 s. The initial C_{pp}s are 0.0025, 0.0033, and 0.004 μS, respectively. (d) Spatiotemporal activity of the network. Each square corresponds to a pyramidal cell. White squares indicate that pyramidal cells are firing. Intervals between frames are 40 ms. (e) Patterns of direction of burst propagation. Wedge-shaped arrows show directions of propagation at locations of pyramidal cells (see Methods). Intervals between frames are 2 s. Directions of propagation vary with time and the network does not show any orderly propagation.

In this way, such vectors were obtained for all bursts of the ith cell during a specific period of time [two seconds in Fig. 2(e) and Fig. 3(e), and five seconds in Fig. 6(e_{viii})] and the vectors were summed. A wedge-shaped arrow at the place of the ith pyramidal cell shows the direction of the summed vector. The length of the summed vector was ignored for clarity of figures. We showed filled circles instead of arrows at edges of the network as correct measurement of the direction was not performed, due to less than eight neighboring pyramidal cells.

III. RESULTS

A. Regulation of spontaneous rhythmic activity by a symmetric STDP function

We examined how STDP influenced the spontaneous rhythmic activity. Values of C_{pp}s were initially uniform over the whole network. Five initial C_{pp}s were tested: 0.0015, 0.0025, 0.0033, 0.004 and 0.005 μS. Figure 2(a) shows the spatial pattern of C_{pp}s in the initial period of 0–20 s ($C_{pp}=0.0033$ μS) before applying STDP algorithm. The size of each filled circle at the locations of pyramidal cells shows the total amount of C_{pp}s from surrounding cells to the corresponding pyramidal cell. The length of each bar initiating from filled circles shows the degree of asymmetry of C_{pp}s (see Methods). Sizes of filled circles are the same and no bar is seen except at the edges because all C_{pp} values are the same.

Each pyramidal cell causes spontaneous bursts of discharges and excites the neighboring pyramidal cells through ERCs. Bursts of action potentials propagate across the CA3 network. Figure 2(d) shows an example of spatial propagation in the network ($C_{pp}=0.0033$ μS). The white squares indicate discharging pyramidal cells. The interval between each panel is 40 ms. Figure 2(e) shows spatial patterns of the direction of propagation. The time scale is longer than that in Fig. 2(d), to show whether persistent pattern of propagation exists or not. Wedge-shaped arrows in each panel show average directions of propagation at places of pyramidal cells every two seconds (See Methods). The patterns of direction differ from each other and do not show any persistent orderly propagation. In other words, propagation occurs irregularly in various directions due to uniform C_{pp}.

Rhythmic activity of the network depends on the C_{pp} value. A larger value of C_{pp} results in a greater number of discharges of pyramidal cells in each burst. As mentioned above, discharges of pyramidal cells are accompanied by the inward Ca^{2+} current through high-threshold Ca^{2+} channels. Although the Ca^{2+} current depolarizes the cells, the increase in the Ca^{2+} concentration inside the cells, in turn, activates

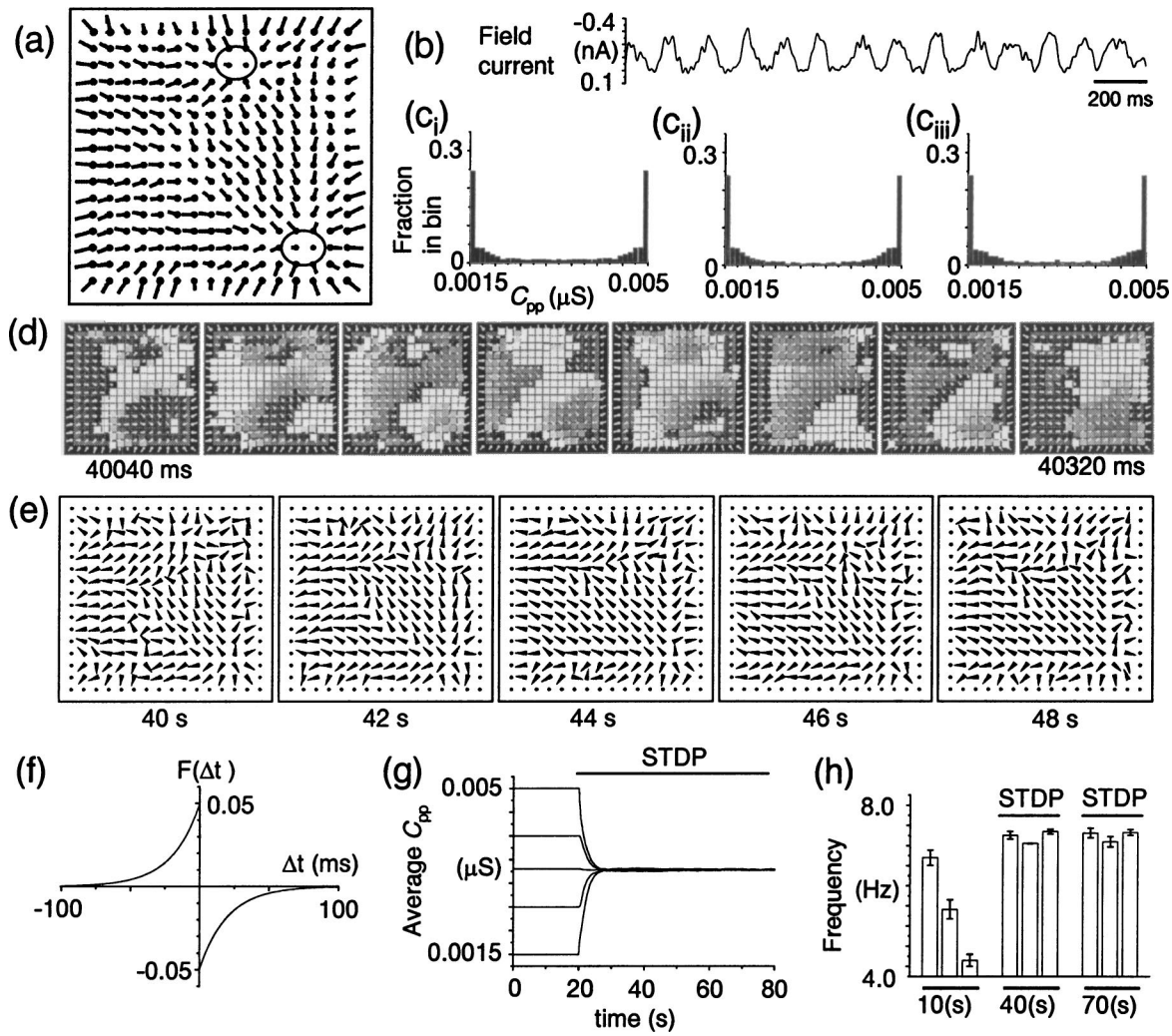

FIG. 3. Spontaneous rhythmic activity after applying STDP algorithm. (a) Spatial pattern of C_{pp}s at 40 s. Two ovals indicate the locations of SORAs that emerge after applying STDP. Note that C_{pp}s from SORAs to the surrounding region are potentiated. (b) Field current obtained from synaptic currents at the center of the network. $(c_i)-(c_{iii})$ Distributions of C_{pp} in the network at 40 s. The initial C_{pp}s are 0.0025, 0.0033, and 0.004 μS, respectively. After applying STDP, the C_{pp} distributions split to upper and lower limits regardless of initial C_{pp}s. (d) Spatiotemporal activity of the network. Each square corresponds to a pyramidal cell. White squares indicate that pyramidal cells are firing. Intervals between frames are 40 ms. Propagation started from SORAs after applying STDP. (e) Patterns of direction of burst propagation. Propagations of burst activity from SORAs to the surrounding region were maintained. (f) STDP function. $T_{bias}=0$. (g) Average C_{pp} over the whole network. Initial C_{pp}s are 0.005, 0.004, 0.0033, 0.0025, and 0.0015 μS from top to bottom. Average C_{pp}s converged to about 0.0033 μS regardless of initial C_{pp}s. (h) Frequencies of the field currents. Three bar charts at 10, 40, and 70 s indicate the mean frequency of the field currents obtained at five different sites in the network for 17 s (3–20 s, 33–50 s, and 63–80 s, respectively); the initial C_{pp}s are 0.0025, 0.0033, and 0.004 μS from left to right at each bar chart. Error bars indicate standard deviation. Rhythmic activity converged to about 7.3 Hz regardless of the initial C_{pp}s.

calcium-activated K^+ channels and the cells are hyperpolarized. The hyperpolarization interrupts discharges and consequently bursts are formed. A greater number of spikes causes higher intracellular Ca^{2+} concentration, which then activates Ca^{2+}-activated K^+ channels more strongly. The membrane potential is eventually hyperpolarized for a longer period of time and the interburst interval increases. On the other hand, a smaller value of C_{pp} causes fewer discharges in each burst and a smaller amount of Ca^{2+} influx. Therefore, larger and smaller C_{pp}s cause longer and shorter interburst intervals, respectively.

To examine the rhythmic activity of the network, we obtained a field current that was defined as the sum of the synaptic currents induced in sixteen pyramidal cells at the central area of the network [Fig. 2(b) and Fig. 3(b)] (see Tateno *et al.* [18] for details about the field current). High-frequency components of the field currents were removed by a low-pass filter (50 Hz cutoff). Figure 2(b) shows thetalike field currents before applying the STDP algorithm; C_{pp} is 0.0033 μS. Peaks of field current oscillations reflect burst discharges of corresponding sixteen pyramidal cells. Larger C_{pp} makes rhythmic activity slower, and smaller C_{pp} makes

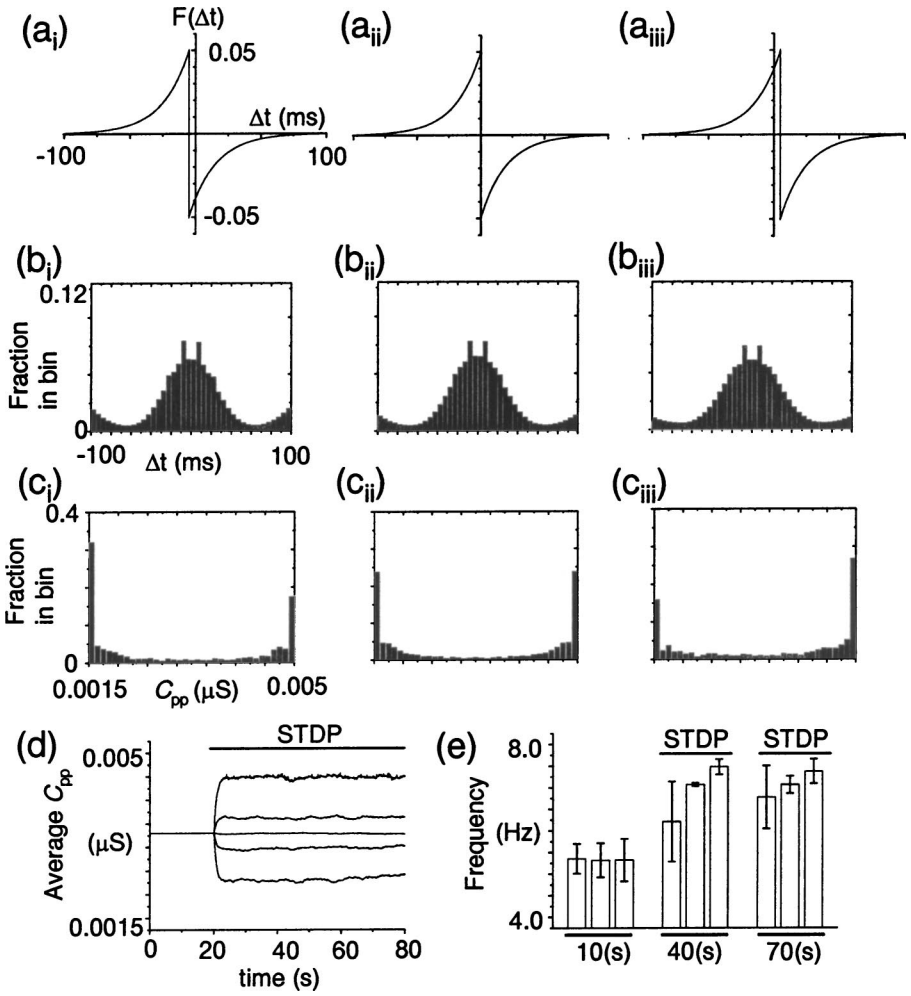

FIG. 4. Regulation of spontaneous rhythmic activity by asymmetric STDP functions. (i)–(iii) The values of T_{bias} are -5, 0, and 5 ms, respectively. (a) STDP functions. (b) Total relative spike timing histogram of all ERC synapses in the network. Total relative spike timing histogram is symmetric regardless of the value of T_{bias}. (c) C_{pp} distribution. Larger value of T_{bias} causes greater number of potentiated ERCs. (d) Average of all C_{pp}s. $T_{bias}=10$, 5, 0, -5, and -10 ms from top to bottom. Converged average C_{pp} depends on T_{bias}. (e) Frequency of the field current. Three bar charts at 10, 40, and 70 s indicate the mean frequency of field currents obtained at five different sites in the network for 17 s (3–20 s, 33–50 s and 63–80 s, respectively); $T_{bias}=5$, 0, -5 ms at each bar chart. Error bars indicate standard deviations. Converged frequency also depends on T_{bias}.

it faster. Tateno *et al.* [18] have shown betalike ($C_{pp}=0.001\ \mu$S), thetalike ($C_{pp}=0.002$ and 0.003 μS) and deltalike ($C_{pp}=0.004$, 0.005 and 0.006 μS) field current rhythms depending on the C_{pp} value. The three bars at ''10 s'' in Fig. 3(h) show the frequencies of the rhythmic activity when C_{pp}s are 0.0025, 0.0033 and 0.004 μS, respectively. The frequency of the principal peak of the power spectrum was measured.

Figures 2(c_i)–(c_{iii}) show the distributions of C_{pp} in the network; C_{pp}s are 0.0025, 0.0033 and 0.004 μS, respectively. Because C_{pp}s are fixed uniformly in the network, each distribution shows only one bar with unity length at corresponding C_{pp}.

C_{pp}s were subject to the STDP function [Fig. 3(f), $T_{bias}=0$] during the period of 20–80 s. Potentiation and depression of C_{pp}s were caused, because pyramidal cells fired in slightly different timing from nearby cells due to propagations of burst activity. Consequently, a distinct spatial pattern of C_{pp} appeared. Figure 3(a) shows the spatial pattern of C_{pp} at 40 s (initially $C_{pp}=0.0033\ \mu$S). There exist two local regions (indicated by ovals) where the sizes of filled circles are smaller than those in the surrounding region, and bars initiating from filled circles in the surrounding region point radially (from ovals to the surrounding region). This indicates that C_{pp}s from the surrounding region to two local regions indicated by ovals are depressed, while C_{pp}s from the local regions to the surrounding region are potentiated. We call such spatial patterns of ERC ''radial ERC.'' Radial ERCs are self-organized at various locations depending on the initial C_{pp}. Bursts of action potentials initiate at the local regions and propagate to the surrounding region along the directions of reinforced C_{pp}s [Fig. 3(d), initially $C_{pp}=0.0033\ \mu$S]. The directions of arrows in Fig. 3(e) show that the burst activity propagates from the two local regions, which correspond to the two local regions in Fig. 3(a). In contrast to Fig. 2(e), the directions of arrows are similar in all panels, indicating that this pattern of propagation is persistent. The local regions thus work as pacemakers of the network. We call this kind of propagation of activity ''radial activity'' and the local regions ''source of radial activity (SORA).''

The average C_{pp} in SORA was about 0.002 μS while the average C_{pp} in the surrounding region was about 0.0033 μS. We estimated frequencies of spontaneous rhythmic activity of pyramidal cells in SORA and the surrounding region, as follows. When C_{pp}s were fixed uniformly at 0.002 μS over the whole network, pyramidal cells caused two to three discharges per burst, resulting in the 8.4 Hz rhythmic activity (data not shown). On the other hand, when C_{pp}s were fixed uniformly at 0.0033 μS over the whole network, pyramidal cells caused three to four discharges per burst, resulting in the 5.7 Hz rhythmic activity. This indicates that pyramidal cells placed in SORA spontaneously cause faster rhythmic

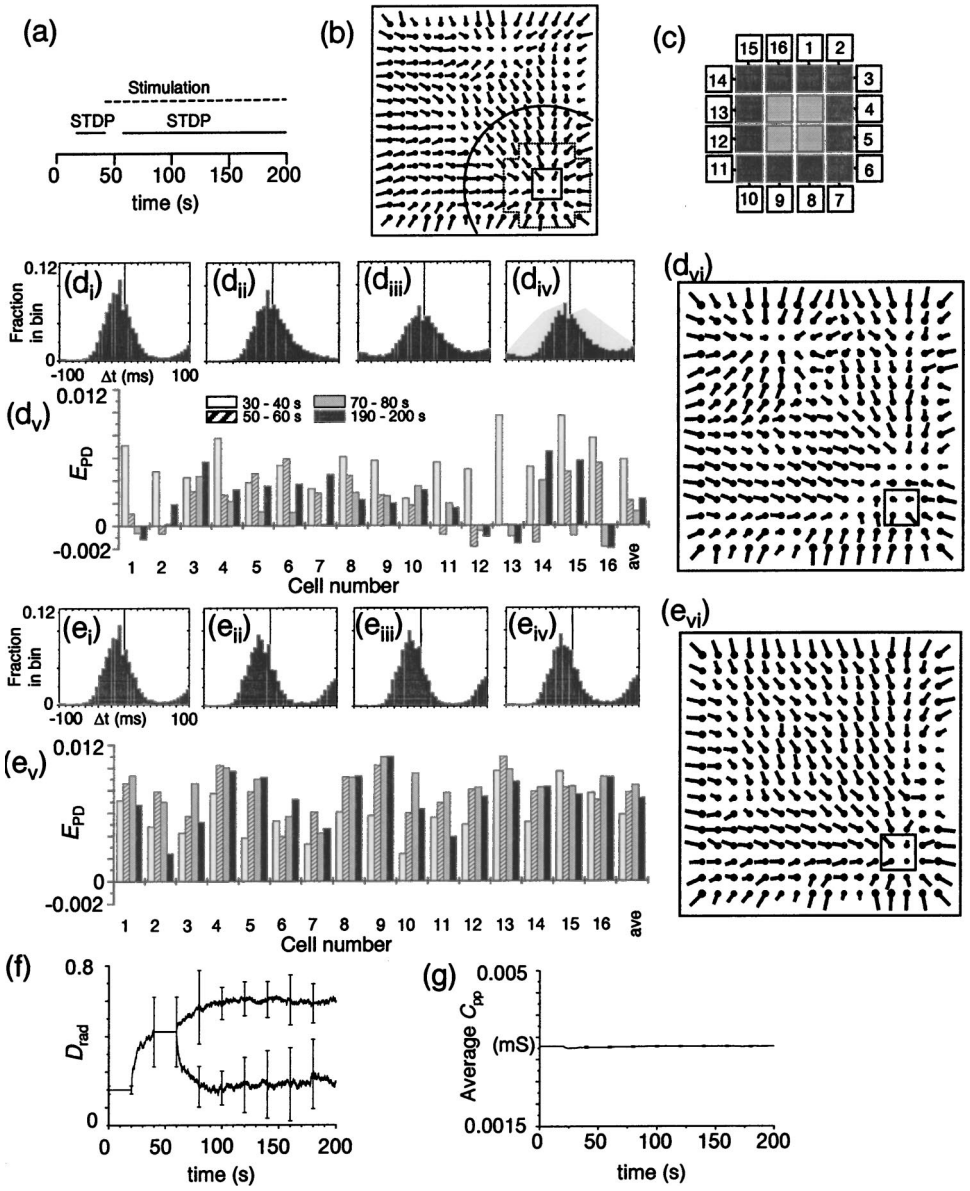

FIG. 5. Input to the self-organized SORAs. (a) Simulation protocol. STDP was applied from 20 to 40 s and from 60 to 200 s (solid lines). Theta burst stimulation was applied from 40 to 200 s (dotted line). (b) Spatial pattern of C_{pp} before applying stimulation. Stimulation was applied to the four pyramidal cells in the small square and the value D_{rad} was evaluated based on the $\mathbf{V}_i$s (see Methods) inside the arc around the stimulus site. The spatial pattern is identical to that in Fig. 3(a). (c) Magnification of the stimulus site that corresponds to the area indicated by dotted lines in Fig. 5(b). Each square corresponds to a pyramidal cell. Four shadowed cells are the stimulated cells. Filled cells are called ''proximal cells'' and numbered cells are called ''distal cells.'' (d) 5 Hz burst stimulation was applied. (e) 8 Hz burst stimulation was applied. (i)–(iv) Average relative spike timing histograms of sixteen synapses from proximal to neighboring distal cells at the intervals of 30–40, 50–60, 70–80, and 190–200 s, respectively. The histogram becomes flat and symmetric by 5 Hz burst stimulation. (v) E_{PD} values of sixteen synapses from proximal to neighboring distal cells. ''ave'' means the average of E_{PD} values of the sixteen synapses. Four E_{PD} values calculated at intervals of 30–40, 50–60, 70–80, and 190–200 s, from left to right, respectively, are shown for each synapse. 5 Hz burst stimulation reduces E_{PD} values significantly. (vi) Spatial pattern of C_{pp} at 200 s. Small square indicates the stimulus site. 5 Hz burst stimulation distorts self-organized radial ERC. (f) Average D_{rad} value as a function of time. Upper and lower branches are the average D_{rad} values during 8 and 5 Hz burst stimulations, respectively. Each branch shows the average taken over six different stimulation sites. Error bars indicate standard deviation. 5 Hz stimulation distorts self-organized radial ERC, and 8 Hz stimulation enhances it. (g) Average of C_{pp}s. Average of all C_{pp}s over the network was obtained for each of twelve simulations (see text). The twelve averages of C_{pp}s were then averaged. Error bars indicate standard deviations. Note that standard deviations are very small because the average C_{pp} is kept almost constant throughout the simulation in every case.

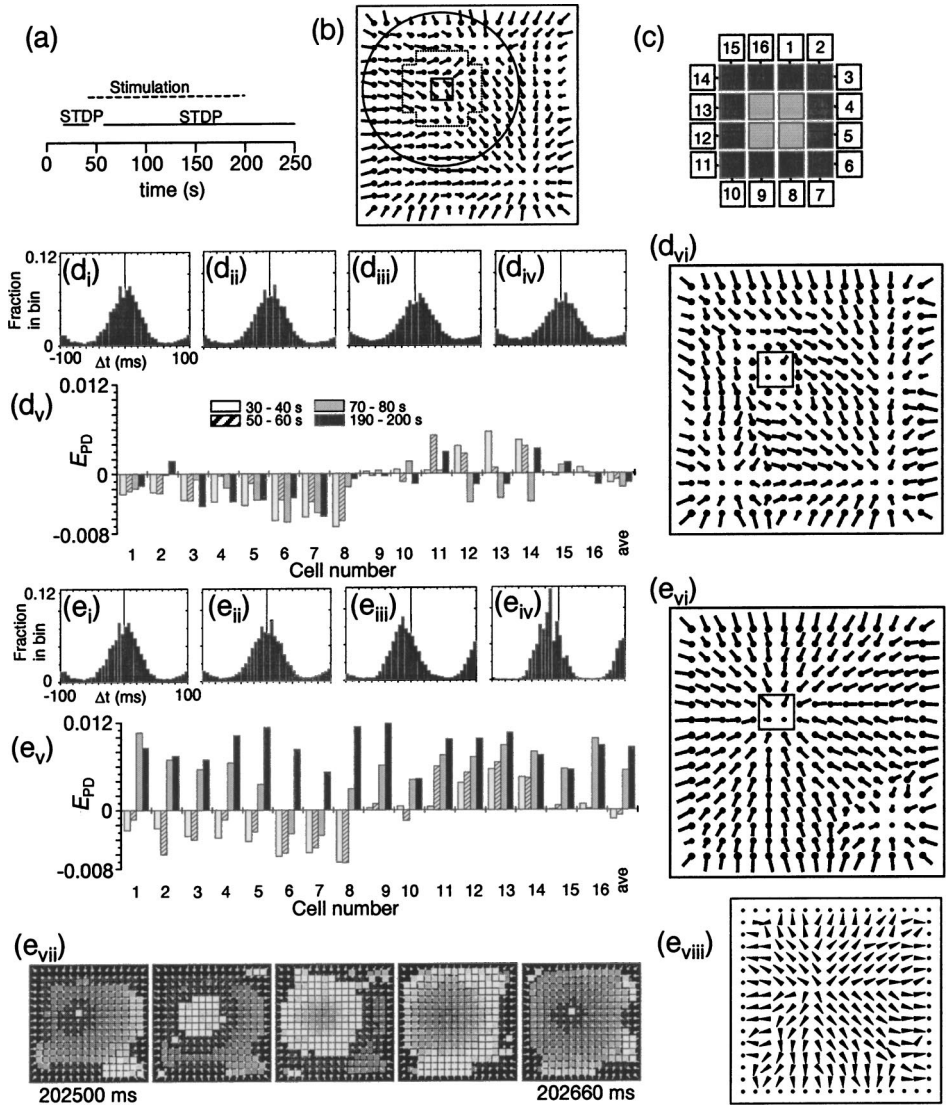

FIG. 6. Input to non-SORA locations. (a) Simulation protocol. STDP was applied from 20 to 40 s and from 60 to 250 s (solid lines). Theta burst stimulation was applied from 40 to 200 s (dotted line). (b) Spatial pattern of C_{pp} before applying stimulation. Stimulation was applied to the four pyramidal cells in the small square and D_{rad} value was evaluated based on the $\mathbf{V}_i$s (see Methods) in the circle around the stimulus site. The spatial pattern is identical to that in Fig. 3(a). (c) Magnification of the stimulus site that corresponds to the area indicated by dotted lines in Fig. 6(b). (d) 5 Hz burst stimulation was applied. (e) 8 Hz burst stimulation was applied. (i)–(iv) Average relative spike timing histogram of sixteen synapses from proximal to neighboring distal cells at the intervals of 30–40, 50–60, 70–80, and 190–200 s, respectively. The histogram gradually shifts to the negative region of Δt and its peak becomes sharper by 8 Hz burst stimulation. (v) E_{PD} values of sixteen synapses from proximal to neighboring distal cells. Four E_{PD} values calculated at intervals of 30–40, 50–60, 70–80, and 190–200 s, from left to right respectively, are shown for each synapse. 8 Hz burst stimulation increases E_{PD} values significantly. (vi) Spatial pattern of C_{pp} at 200 s. 8 Hz burst stimulation organizes a new radial ERC. (vii) Spatiotemporal activity of the network just after quitting stimulation (around 202.5 s). Activity propagating from the new SORA is clearly seen. (viii) Spatial pattern of direction of burst propagation in the period of 200–205 s.

activity than that in the other region. As a result, SORA may act as a pacemaker, generating bursts of discharges in advance of the surrounding region. Since burst activity starts in SORA and propagates to the surrounding region, ERCs from cells in SORA to cells in the surrounding region are strengthened through STDP. On the other hand, ERCs from cells in the surrounding region to cells in SORA are weakened. C_{pp}s in SORA are therefore kept small and SORA can keep acting as a pacemaker. As a consequence, radial activity is maintained.

Distribution of C_{pp} values split into two groups near the upper and lower limits due to generation of radial ERCs [Figs. $3(c_i)-3(c_{iii})$]. This distribution was almost the same, irrespective of initial C_{pp}s and the spatial pattern of C_{pp}s organized through STDP. The average C_{pp} value in the network therefore converged to about 0.0033 μS from five dif-

ferent values of initial C_{pp}s irrespective of initial C_{pp}s [Fig. 3(g)].

Rhythmic activity that depended on initial C_{pp} gradually converged to a theta-like rhythm with the main frequency component at 7.3 Hz, as the average C_{pp} converged to about 0.0033 μS [Fig. 3(h)]; initial C_{pp}s were 0.0025, 0.0033, and 0.004 μS from the left to the right at each time. Figure 3(b) shows example of theta-like field current rhythm around 40 s (initially $C_{pp}=0.0033$ μS). Spontaneous rhythmic activity is thus regulated by STDP.

When C_{pp}s were initially 0.0033 μS, the consequent average C_{pp} was almost the same as the initial C_{pp}. The consequent frequency of rhythmic activity (7.3 Hz) was, however, significantly higher than the initial frequency (5.7 Hz) [compare middle bars at 10 and 70 s in Fig. 3(h)]. The consequent frequency (7.3 Hz) is close to the estimated frequency of spontaneous rhythmic activity of pyramidal cells in SORA (8.4 Hz). This shows that the effect of SORAs as pacemakers of the network is very strong.

B. Regulation of spontaneous rhythmic activity by asymmetric STDP functions

Experimentally observed STDP functions depend on brain tissues and preparations. It is interesting to examine how radial-activity and regulation of rhythmic activity rely on the shape of the STDP function. There are several parameters that modify the STDP function: for example, locations of positive and negative peaks, height of the peaks, and shape of the tails. There is a distinct difference between the STDP functions that have been observed in dissociated and cultured hippocampal cells by Bi and Poo [16] and in cultured CA3 slices by Debanne *et al.* [15]. While the STDP function observed by Bi and Poo [16] induces neither LTP nor LTD when pre- and postsynaptic cells fire at the same time ($\Delta t=0$), the STDP function observed by Debanne *et al.* [15] induces LTD at $\Delta t=0$. In this section, we therefore focus on the locations of the peaks. The peaks of the STDP function were shifted by changing the value of the parameter T_{bias}: -10, -5, 0, 5, and 10 ms [Figs. $4(a_i)-(a_{iii})$ for $T_{bias}=-5$, 0, and 5 ms, respectively]. Negative and positive values of T_{bias} induced depression and potentiation at $\Delta t=0$, respectively.

Simulations were started with the same initial value of C_{pp} (0.0033 μS, uniform over the whole network). Figures $4(b_i)-4(b_{iii})$ show the total relative spike timing histograms of all ERC synapses obtained after the average value of C_{pp} has converged (35–50 s) using STDP functions in Fig. $4(a_i)-4(a_{iii})$, respectively. The relative spike timing histograms that show how often pre- and postsynaptic spikes occur at an interval of Δt all over the network are symmetric regardless of the values of T_{bias} because the network has recurrent connections. When pre- and postsynaptic pyramidal cells, i and j, fire at an interval of Δt_{ij}, pyramidal cells, j and i, fire at the interval of $-\Delta t_{ij}$. In the present model, if there is a synaptic connection from cell i to cell j, then there is a synaptic connection from cell j to cell i. Thus, each pair of firings equally contributes to the total relative spike timing histogram at Δt_{ij} and $-\Delta t_{ij}$, assuring a symmetric histogram.

When T_{bias} is 0 ms, the STDP function [Fig. $4(a_{ii})$] and the relative spike timing histogram [Fig. $4(b_{ii})$] are both symmetric. This indicates that the numbers of potentiated and depressed synapses are equal. In fact, the distribution of the C_{pp} value in the network shows two peaks with the same height at the upper and lower limits of C_{pp} [Fig. $4(c_{ii})$ as well as Fig. $3(c_{ii})$]. This split distribution of C_{pp} allows formation of radial ERCs, as shown in the previous section [Fig. 3(a)]. When the values of T_{bias} are -5 and 5 ms, STDP functions are shifted to the left and right [Figs. $4(a_i)$ and $4(a_{iii})$], and depression and potentiation occur respectively at more synapses [Figs. $4(c_i)$ and $4(c_{iii})$]. Despite the excess number of depressed or potentiated synapses, radial ERCs appear and radial-activities occur (not shown).

When the values of T_{bias} are -10 and 10 ms, almost all the synapses are depressed and potentiated, respectively (not shown). C_{pp}s are spatially symmetric at most locations in the network because either depressed or potentiated synapses dominate. Radial ERCs are therefore hardly formed in these cases. Propagation directions are irregular, as observed in the network with uniform C_{pp}s (not shown). Assuming that information is stored as spatial patterns of potentiated and depressed C_{pp}s in CA3, almost no information can be stored in these cases. On the other hand, $T_{bias}=0$ would maximize the ability to store information.

Traces in Fig. 4(d) are time courses of the average of all C_{pp}s at $T_{bias}=10$, 5, 0, -5, and -10 ms, from top to bottom, respectively. The average of all C_{pp}s reflects the distribution of C_{pp} [Figs. $4(c_i)-4(c_{iii})$]. Figure 4(e) shows a change of the frequency of the rhythmic activity. The height of the three bars at each time shows the frequency of the rhythmic activities at $T_{bias}=-5$, 0, and 5 ms, from left to right, respectively. The rhythmic activity converges to a frequency depending on the average C_{pp} value. As the value of T_{bias} increases, the frequency becomes lower because the average C_{pp} value becomes larger.

C. Rise and fall of the self-organized radial activity by burst stimulation

The hippocampal CA3 region receives input signals from the dentate gyrus through mossy fibers. We examined how input signals influenced self-organized radial activity of the CA3 network. The theta rhythm (4–10 Hz) has been observed in the dentate gyrus, and the majority of granule cells fire in bursts phase locked to the theta rhythm [26]. We therefore applied theta burst stimuli to the present CA3 model.

An interesting issue related to the theta frequency is the phase precession of place cell activity. When rats enter into a specific place field, the firing phase of the corresponding place cells gradually proceeds from late to early phase of the major theta activity [7,27]. This means that the firing frequency of place cells is slightly higher than that of the other cells. We therefore used 8 Hz burst stimulation whose frequency was higher than the frequency of spontaneous rhythmic activity. Since the frequency of spontaneous rhythmic activity of the present model depended on the value of T_{bias} as shown in the previous section, STDP function with $T_{bias}=0$ was used, which led the spontaneous frequency to about

7 Hz. 5 Hz burst stimulation was also used in order to compare the responses with the responses to the 8 Hz stimulation.

Figure 5(a) shows simulation protocols. The solid and dotted lines indicate the periods where STDP is effective and stimulation is applied, respectively. This protocol is the same as that in Sec. III A until stimulus onset (up to 40 s). The initial conditions of the network are also the same as in Sec. III A. Therefore, the spatial pattern of C_{pp}s in Fig. 5(b) is identical to that in Fig. 3(a) before applying stimulation. STDP was frozen temporarily (from 40 to 60 s) and C_{pp}s were fixed in order to investigate the effects of stimulation itself on the network activity.

Four pyramidal cells located at the center of one of the self-organized SORAs, indicated by the small square in Fig. 5(b), were stimulated simultaneously by 5 or 8 Hz burst stimulation (3 pulses in each burst, interpulse interval $=10$ ms, interburst interval$=200$ or 125 ms). Figure 5(c) is the magnification of the SORA indicated by dotted lines in Fig. 5(b). The central four cells indicated by shadowed squares correspond to the stimulated cells. We call numbered cells (1–16) ''distal cells'' (distal to the stimulus site) and filled cells ''proximal cells'' (proximal to the stimulus site).

The relative spike timing histograms at sixteen synapses from proximal cells to their closest distal cells were obtained (data not shown). Lines between distal cells and proximal cells in Fig. 5(c) indicate these synaptic connections. Figures $5(\mathrm{d_i})$ and $5(\mathrm{e_i})$ show the average of the sixteen relative spike timing histograms before applying stimulation (30–40 s). Since the spontaneous activity propagates from self-organized SORA to the surrounding region with a theta cycle as shown in Sec. III A, the proximal cells fire earlier than the distal cells. This results in the peak of the average relative spike timing histogram being in the negative range of Δt.

White bars in Figs. $5(\mathrm{d_v})$ and $5(\mathrm{e_v})$ show values of E_{PD} (see Methods) for the sixteen synapses from proximal to distal cells before applying stimulation. The E_{PD} values were calculated from each of the sixteen relative spike timing histograms and the STDP function [Fig. 3(f)]. They are all positive, indicating that all of the sixteen synaptic connections from the proximal to the distal pyramidal cells are potentiated ($\approx C_{max}$) by radial-activity. On the other hand, the synaptic connections in the opposite direction (from the distal to the proximal cells) are depressed ($\approx C_{min}$).

5 Hz burst stimulation

When SORA was stimulated by 5 Hz bursts and STDP was frozen, pyramidal cells in SORA caused 5 Hz bursts of discharges due to the stimulation, while cells in the surrounding region showed 7 Hz bursts of discharges spontaneously. As a result, burst activity initiated more often in the surrounding region than in SORA and propagated toward SORA. The average relative spike timing histogram was broadened and the peak shifted toward the center [Fig. $5(\mathrm{d_{ii}})$]. This indicates that the burst propagation from the proximal to distal cells becomes less prominent. Most of the E_{PD} values (striped bars) thus became smaller than those before stimulus onset (white bars), as shown in Fig. $5(\mathrm{d_v})$, and some synapses showed negative E_{PD} values. Although depression of C_{pp}s does not occur because STDP is frozen, the negative E_{PD} values indicate that depression may occur once STDP is resumed.

When STDP was resumed, the relative spike timing histogram was broadened further and became almost symmetric by the 5 Hz burst stimulation, as shown in Figs. $5(\mathrm{d_{iii}})$ and $5(\mathrm{d_{iv}})$. The average E_{PD} value became smaller as shown in Fig. $5(\mathrm{d_v})$ (compare white and black bars at ''ave''). These reflect the distortion of radial activity. Figure $5(\mathrm{d_{vi}})$ shows the spatial pattern of C_{pp} at 200 s. Some of the bars around the stimulus site do not point in radial directions, showing that radial ERC is distorted.

8 Hz burst stimulation

When 8 Hz burst stimulation was applied, pyramidal cells in SORA showed 8 Hz bursts of discharges due to the stimulation. Because 8 Hz was higher than the spontaneous burst frequency, propagation of burst discharges occurred more frequently from SORA. The peak of the relative spike timing histogram was always in the negative region of Δt [Figs. $5(\mathrm{e_i})$–$5(\mathrm{e_{iv}})$] and the average E_{PD} value increased as shown in Fig. $5(\mathrm{e_v})$ (compare white and black bars at ''ave''). This indicates that propagation from SORA occurs more frequently by the 8 Hz burst stimulation, and radial ERC is not destroyed [Fig. $5(\mathrm{e_{vi}})$].

Stimuli to different SORAs

The locations of self-organized radial-activities depend on the initial conditions, such as initial membrane potentials of pyramidal cells and interneurons. Three different sets of initial membrane potentials for 256 pyramidal cells were prepared by randomly choosing the initial membrane potential for each pyramidal cell. As a result, two to three radial activities were organized at different locations depending on the initial conditions (not shown). Two of the major SORAs were chosen as stimulus sites for each initial condition (a total of six different SORAs was chosen). Each of the six SORAs was stimulated first by 5 Hz burst, and then by 8 Hz burst. Four pyramidal cells at each SORA were stimulated simultaneously.

In this way, each of 5 and 8 Hz burst stimuli was applied to six different self-organized SORAs. Enhancement and distortion of radial ERC were measured by the value D_{rad} (see Methods). The black arc in Fig. 5(b) shows the area in which the value D_{rad} is calculated when four pyramidal cells in the small square are stimulated. Upper and lower traces in Fig. 5(f) show average time courses of the six D_{rad} values when 8 and 5 Hz stimuli are applied respectively. Error bars indicate standard deviations. The value of D_{rad} increases immediately by 8 Hz stimulation and decreases by 5 Hz stimulation. Radial-ERC is therefore enhanced by 8 Hz burst stimulation and depressed by 5 Hz stimulation regardless of the location of the self-organized radial activity.

We obtained the average of all C_{pp}s for all twelve simulations [Fig. 5(g)]. Error bars that show standard deviations are very small and almost impossible to see. The average C_{pp}

is always constant, indicating that stimulation does not affect the total amount of C_{pp}s under regulation by STDP.

D. Organization of radial activity by burst stimulation

8 Hz burst stimulation to a self-organized SORA preserved radial activity, while 5 Hz burst stimulation distorted it, as mentioned in the previous section. We next investigated whether burst stimulation to a site in the non-SORA region organized a new radial activity. The simulation protocol was the same as in the previous section, but burst stimulation was terminated at 200 s, as shown in Fig. 6(a), to investigate the network activity after the termination of the stimulation.

Since initial conditions of the network are the same as in Sec. III A, the spatial pattern of C_{pp}s in Fig. 6(b) is the same as those in Fig. 3(a) and 5(b) before applying stimulation. Figure 6(c) is the magnification of the area indicated by dotted lines in Fig. 6(b); the central four neurons indicated by shadowed squares are stimulated.

As spontaneous activity propagates from the two self-organized SORAs to the surrounding region, the activity propagates frequently from right to left around the stimulus site before applying stimulation [see Figs. 3(d) and 3(e)]. The relative spike timing histograms at the synapses from the proximal cells to the distal cells 1–8 show a peak in the positive range of Δt, while the histograms of synapses from proximal to other distal cells (9–16) show a peak in the negative range (not shown), reflecting the propagation approximately from right to left. The average relative spike timing histogram at sixteen synapses on the cells 1–16 therefore shows sharp peaks in both positive and negative ranges of Δt as shown in Figs. $6(d_i)$ and $6(e_i)$. However, neither of the peaks dominates the histogram, and the histogram is almost symmetric. This means that the stimulus site is neither a strong source nor a sink of propagation before applying stimulation. E_{PD} values of the synapses from the proximal cells to the distal cells 1–8 are negative, while the synapses from proximal to other distal cells (9–16) show positive E_{PD} values [white bars in Figs. $6(d_v)$ and $6(e_v)$]. This depends on the peaks of the relative spike timing histograms in the negative and positive Δt ranges (not shown). These values indicate that synapses from the proximal to the distal cells are potentiated in the left hand side of the stimulus site, while those in the other side are depressed.

5 Hz burst stimulation

Figures $6(d_{ii})$–$6(d_{iv})$ are the average relative spike timing histograms during 5 Hz burst stimulation. Neither of the sharp peaks in the histograms grows and the shape of the histograms remains almost the same. E_{PD} value of each synapse changes with time [striped, shadowed, and black bars in Fig. $6(d_v)$] but the average E_{PD} value is always small. This indicates that the direction of the propagation around the stimulus site changes occasionally during stimulation but radial activity from the stimulus site does not occur. This is because the frequency of the spontaneous rhythmic activity (about 7 Hz) is higher than that of the burst stimulation (5 Hz). 5 Hz burst stimulation does not organize a new radial ERC [Fig. $6(d_{vi})$].

8 Hz burst stimulation

Figures $6(e_{ii})$–$6(e_{iv})$ show the average relative spike timing histograms during 8 Hz stimulation. While the peak in the positive range of Δt disappears with time, the peak in the negative range grows [Fig. $6(e_{iii})$]. The peak in the negative range moves slightly to the negative side and becomes sharper [Fig. $6(e_{iv})$]; the histogram is no longer symmetric. E_{PD} values gradually increase and all of them become positive in the period of 190–200 s [black bars in Fig. $6(e_v)$]. This indicates that the propagation of the spontaneous bursts from right to left around the stimulus site turns into a radial activity from the stimulus site. As a result, a new radial ERC is organized [Fig. $6(e_{vi})$]. Figure $6(e_{vii})$ shows the spatiotemporal activity of the network about 2.5 s after quitting stimulation. Figure $6(e_{viii})$ shows average directions of propagation in the period of 200–205 s. Propagation of burst activity from the new SORA to the surrounding region is clearly seen.

Stimuli to different sites in the non-SORA region

We verified different effects of 5 and 8 Hz burst stimulation by applying 5 or 8 Hz stimulation to eight more different sites in the non-SORA region (not shown). Initial conditions were the same for all the cases. Organization of radial ERC was measured by the value D_{rad} as in the previous section. Upper and lower traces in Fig. 7(a) show average time courses during 8 and 5 Hz stimulations, respectively. Error bars indicate standard deviations. Before applying stimulation, the average D_{rad} value is lower than that in Fig. 5(f) because we choose stimulus sites in the non-SORA region. The D_{rad} value starts increasing by 8 Hz stimulation and takes about 100 s to reach the maximum. 5 Hz stimulation, on the other hand, decreased the D_{rad} value slowly. This suggests that the above different effects of 5 and 8 Hz burst stimulation do not depend on the stimulus site in the non-SORA region.

Radial-ERC fades away after the termination of the 8 Hz burst stimulation. The D_{rad} value, 10 s after the termination of the stimulation, decreases to 80% of the value at 200 s [Fig. 7(b)]. Average C_{pp} is constant, as in the previous section, even after the termination of the stimulation [Fig. 7(c)]. This indicates that the total amount of C_{pp}s is maintained regardless of stimulation.

IV. DISCUSSION

We found that the frequency of spontaneous rhythmic activity of the CA3 network model converged into a specific frequency depending on the shape of the STDP function. We also found that burst stimulation to a local site of the CA3 network model was able to organize a new radial ERC, though the radial ERC decayed gradually after the stimulation was terminated. This suggests that memory traces may be stored for a while as radial activities coexisting with spontaneous rhythmic activity. Moreover, we found that stimulation whose frequency was higher than that of the spontaneous rhythm organized radial activity, while lower frequency stimulation did not.

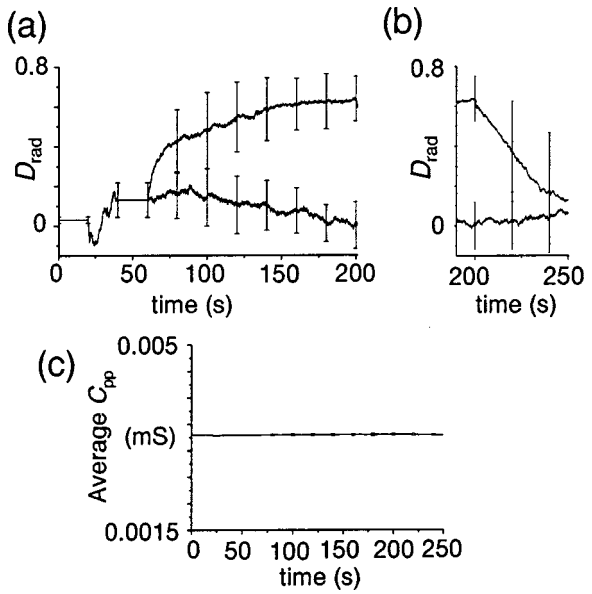

FIG. 7. Degree of radial ERC and average C_{pp} as a function of time. Non-SORA locations were stimulated. (a) Average D_{rad} value as a function of time. Upper and lower branches are the average D_{rad} values during 8 and 5 Hz burst stimulations, respectively. Each branch shows the average taken over nine different stimulation sites. 8 Hz stimulation organizes a new radial ERC while 5 Hz stimulation does not, regardless of the stimulation site. (b) Average D_{rad} value as a function of time after stimulation was terminated. Radial ERC is preserved for several seconds. (c) Average of C_{pp}s. Average of all C_{pp}s over the network was obtained for each of eighteen simulations (see text). The eighteen averages of C_{pp}s were then averaged. Error bars indicate standard deviations. Note that standard deviations are very small because the average C_{pp} is kept almost constant throughout the simulation in every case.

If memories are stored in CA3 by potentiated synaptic conductances without depression of other synaptic conductances, CA3 would lose the stability of theta activity when multiple memory patterns are stored. In fact, LTP caused by tetanic stimulation leads CA3 to epileptic spontaneous activity [28]. The fact that memory storage does not induce epilepsy implies the existence of a mechanism that regulates the excitability of the network. Our results show that STDP is a candidate for this regulation mechanism.

Regulation of neural activity is one of the most interesting issues related to STDP. Using a single integrate-and-fire neuron model, Song *et al.* have shown that the firing rate of the neuron is regulated because the membrane potential of the neuron is maintained near the firing threshold by STDP [23]. This leads the neuron to maintain sensitivity to synaptic input. Although regulation of neural activity of a network model has also been reported by other authors [25], mechanisms of network activity regulation have not been understood clearly. It is an interesting issue whether mechanisms of activity regulation of a single neuron shown by Song *et al.* [23] can be underlying mechanisms of activity regulation of neural networks such as CA3, where multiple neurons are recurrently connected.

Our results show that the STDP function with equal LTP and LTD areas can regulate the frequency of spontaneous activity. This is due to the existence of recurrent connections. In our model, each pyramidal cell sends synaptic signals to nearby cells and also receives synaptic signals from them [Fig. 1(a)]. If relative spike timing at a synapse from pyramidal cell i to pyramidal cell j is Δt_{ij}, then relative spike timing at a synapse from cell j to cell i is $-\Delta t_{ij}$. In this way, discharges of cell i and cell j contribute to make the total relative spike timing histogram symmetric as mentioned above. The total relative spike timing histogram is actually symmetric regardless of the activity of the network and the shape of the STDP function [Fig. 4(b)]. Therefore, the STDP function with equal LTP and LTD areas ($T_{bias}=0$ ms) induced the same amount of potentiated and depressed synapses [Fig. $4(c_{ii})$].

Song *et al.*, on the other hand, have reported that the LTD area of the STDP function has to surpass the LTP area to cause a similar number of potentiated and depressed synapses [23]. The major reason for this would be the lack of recurrent connections in their model. Their model is a single neuron with a number of afferent connections. In such a model, synaptic connections from precells to one postcell exist but the opposite synaptic connections do not exist. Discharges of precells i and one postcell j, therefore, contribute to the total relative spike timing histogram only at Δt_{ij}. Moreover, because discharges of the precells i contribute to discharges of the one postsynaptic cell j, Δt_{ij} would be negative more often. The total relative spike timing histogram would then be asymmetric and distribute more in the negative range of Δt. This indicates that if a STDP function with equal LTP and LTD area [such as Fig. $4(a_{ii})$] is used, the majority of synapses would be potentiated. In other words, the STDP function with a larger LTD area would be necessary to compensate the asymmetric relative spike timing in Song's model.

Sustained post-stimulus activity has been observed in a delay-nonmatch-to-sample paradigm in rats [29], suggesting that stimulus dependent activity may be preserved in the CA3 region of the real hippocampus in a short period of time. The source of propagation was preserved for about 10 s after the termination of stimulation in our model [Fig. 7(b)]. Although this period of time is relatively short compared to the period of time necessary to organize radial-activity, this period of time might be enough to link current information to subsequent information that will come into CA3.

The relatively short duration of newly created radial activities probably results from the network geometry. As mentioned above, edges of this network receive fewer synaptic inputs than the other regions. Although the edge effects were reduced by modification of g_{af} (see Methods), radial activities tended to be organized spontaneously near the edges. These self-organized radial activities were difficult to destroy completely. In fact, when a new radial ERC was organized by burst stimulation as shown in Sec. III D [Fig. $6(e_{vi})$], a self-organized radial ERC at the lower right corner still existed even though it was very small compared to the newly organized radial ERC. When stimulation was terminated, this small self-organized radial ERC started to grow and gradually destroyed the newly organized radial ERC. Con-

taining only 256 pyramidal cells, our network model is smaller than the real CA3 region. Enlarging the network size would reduce the edge effects, and newly organized radial activities might last longer.

ACKNOWLEDGMENTS

We thank Dr. K. Nakashima and Dr. K. Tateno for useful comments on the work, and D. Tabizel for linguistic help on the manuscript. This work was supported by the Ministry of Education (Grants-in-Aid for Scientific Research, No. 14580425 and No. 15016084).

APPENDIX A

Rate constants of ion gates and parameter values of the CA3 pyramidal cell model are as follows:

$$\alpha_m=\frac{-0.32(51.9+V)}{\exp(-(51.9+V)/4)-1},\quad \beta_m=\frac{0.28(V+24.9)}{\exp((V+24.9)/5)-1},$$

$$\alpha_h=0.128\exp\left(\frac{-48-V}{18}\right),\quad \beta_h=\frac{4}{1+\exp(-(25+V)/5)},$$

$$\alpha_s=\frac{0.2}{1+\exp(-0.072V)},\quad \beta_s=\frac{0.0025(V+13.9)}{\exp((V+13.9)/5)-1},$$

$$\alpha_r=\begin{cases}\dfrac{\exp(-(V+65)/20)}{1600} & (V>-65),\\ 0.000625 & (V\leqslant -65),\end{cases}$$

$$\beta_r=\begin{cases}\dfrac{0.005-8\alpha_r}{8} & (V>-65),\\ 0 & (V\leqslant -65),\end{cases}$$

$$\alpha_{s(low)}=\frac{1.6}{1+\exp(-0.072(V+40))},$$

$$\beta_{s(low)}=\frac{0.02(V+53.9)}{\exp((V+53.9)/5)-1},$$

$$\alpha_{r(low)}=\begin{cases}\dfrac{\exp(-(V+105)/20)}{200} & (V>-105),\\ 0.005 & (V\leqslant -105),\end{cases}$$

$$\beta_{r(low)}=\begin{cases}0.005-\alpha_{r(low)} & (V>-105),\\ 0 & (V\leqslant -105),\end{cases}$$

$$\alpha_n=\frac{-0.016(29.9+V)}{\exp(-(29.9+V)/5)-1},\quad \beta_n=0.25\exp\left(\frac{-45-V}{40}\right),$$

$$\alpha_a=\frac{-0.02(51.9+V)}{\exp(-(51.9+V)/10)-1},$$

$$\beta_a=\frac{0.0175(V+24.9)}{\exp((V+24.9)/10)-1},$$

$$\alpha_b=0.0016\exp\left(-\frac{V+78}{18}\right),\quad \beta_b=\frac{0.05}{1+\exp(-(54.9+V)/5)},$$

$$\alpha_q=\begin{cases}0 & [(\chi-140)<0],\\ 0.00002(\chi-140) & [0\leqslant(\chi-140)<500],\\ 0.01 & [500\leqslant(\chi-140)],\end{cases}$$

$$\beta_q=0.001,$$

$$\alpha_c=\begin{cases}\dfrac{\exp((V+55)/11-(V+58.5)/27)}{18.975} & (V\leqslant -15),\\ 2\exp\left(\dfrac{-58.5-V}{27}\right) & (V>-15),\end{cases}$$

$$\beta_c=\begin{cases}2\exp\left(\dfrac{-58.5-V}{27}\right)-\alpha_c & (V\leqslant -15),\\ 0 & (V>-15),\end{cases}$$

$$C=0.1\ (\mu\mathrm{F}),\ g_{Na}=1.0,\ g_{Ca}=0.13,$$

$$g_{Ca(low)}=0.03,\ g_{K(DR)}=0.08,\ g_{K(A)}=0.17,\ g_{K(AHP)}=0.07,$$

$$g_{K(C)}=0.366,\ g_L=0.0033,\ g_{af\ center}=0.005,$$

$$g_{af\ edge}=0.004,\ g_{af\ center}=0.003(\mu\mathrm{S}).$$

$$V_{Na}=50,\ V_{Ca}=75,\ V_K=-80,\ V_L=-65,$$

$$V_{syn(e)}=-10(\mathrm{mV}),\ \phi=50,\ \beta_\chi=0.075(\mathrm{ms}^{-1}).$$

Rate constants of ion gates and parameter values of the interneuron model are as follows:

$$\alpha_m=\frac{-0.64(51.9+V)}{\exp(-(51.9+V)/4)-1},\quad \beta_m=\frac{0.56(V+24.9)}{\exp((V+24.9)/5)-1},$$

$$\alpha_h=\frac{0.128\exp(-(48+V)/18)}{0.65},$$

$$\beta_h=\frac{4}{0.65(1+\exp[-(25+V)/5])},$$

$$\alpha_n=\frac{-0.016(48.9+V)}{0.65(\exp[-(48.9+V)/5]-1)},$$

$$\beta_n=\frac{0.25\exp(-(64+V)/40)}{0.65},$$

$$C=0.1(\mu\mathrm{F}),\ g_{Na}=1.5,\ g_{K(DR)}=0.3,\ g_L=0.02(\mu\mathrm{S}),$$

$$V_{Na}=50,\ V_K=-80,\ V_L=-65(\mathrm{mV}).$$

APPENDIX B

The parameter values in Eqs. (6) and (7) are as follows:

$$C_{pp}=0.0015-0.005(\text{depending on each synapse}),$$

$$C_{pi}=0.02,\ C_{ip}=0.01,\ C_{stim}=0.05(\mu S),\qquad \tau_{1(pp)}=\tau_{1(ip)}=\tau_{1(stim)}=3,\ \tau_{1(pi)}=1,$$

$$V_{pp}=V_{pi}=V_{stim}=-10,\ V_{ip}=-70(mV),\qquad \tau_{2(pp)}=\tau_{2(ip)}=\tau_{2(stim)}=2,\ \tau_{2(pi)}=0.5(ms).$$

[1] N. Tamamaki and Y. Nojyo, J. Comp. Neurol. **303**, 435 (1991).
[2] X.-G. Li, P. Somogyi, A. Ylinen, and G. Buzsáki, J. Comp. Neurol. **339**, 181 (1994).
[3] D. Marr, Philos. Trans. R. Soc. London, Ser. B **262**, 23 (1971).
[4] B. L. McNaughton and G. M. Morris, Trends Neurosci. **10**, 408 (1987).
[5] A. Treves and E. T. Rolls, Hippocampus **4**, 374 (1994).
[6] J. O'keefe and L. Nadel, *The Hippocampus as a Cognitive Map* (Clarendon, Oxford, UK, 1978).
[7] W. E. Skaggs, B. L. McNaughton, M. A. Wilson, and C. A. Barnes, Hippocampus **6**, 149 (1996).
[8] K. Nakazawa, M. C. Quirk, R. A. Chitwood, M. Watanabe, M. F. Yeckel, L. D. Sun, A. Kato, C. A. Carr, D. Johnston, M. A. Wilson, and S. Tonegawa, Science **297**, 211 (2002).
[9] G. Buszźki, Neuron **33**, 325 (2002).
[10] F. Strata, Hippocampus **8**, 666 (1998).
[11] B. Kocsis, A. Bragin, and G. Buzsáki, J. Neurosci. **19**, 6200 (1999).
[12] C. Wu, H. Shen, W. P. Luk, and L. Zhang, J. Physiol. (London) **540**, 509 (2002).
[13] J. C. Magee and D. Johnston, Science **275**, 209 (1997).
[14] H. Markram, J. Lubke, M. Frotscher, and B. Sakmann, Science **275**, 213 (1997).
[15] D. Debanne, B. H. Gahwiler, and S. M. Thompson, J. Physiol. (London) **507**, 237 (1998).
[16] G. Bi and M. Poo, J. Neurosci. **18**, 10464 (1998).
[17] M. Nishiyama, K. Hong, K. Mikoshiba, M. Poo, and K. Kato, Nature (London) **408**, 584 (2000).
[18] K. Tateno, H. Hayashi, and S. Ishizuka, Neural Networks **11**, 985 (1998).
[19] D. A. Brown and W. H. Griffith, J. Physiol. (London) **337**, 303 (1983).
[20] Y. Kawaguchi and K. Hama, Brain Res. **411**, 190 (1987).
[21] Y. Kawaguchi, H. Katsumaru, T. Kosaka, C. W. Heizmann, and K. Hama, Brain Res. **416**, 369 (1987).
[22] R. Miles, J. Physiol. (London) **428**, 61 (1990).
[23] S. Song, K. D. Miller, and L. F. Abbott, Nat. Neurosci. **3**, 919 (2000).
[24] N. Levy, D. Horn, I. Meilijson, and E. Ruppin, Neural Networks **14**, 815 (2001).
[25] K. Kitano, H. Câteau, and T. Fukai, Neurocomputing **44**, 473 (2002).
[26] M. D. Muñoz, A. Núñez, and E. García-Austt, Brain Res. **509**, 91 (1990).
[27] J. O'Keefe and M. L. Recce, Hippocampus **3**, 317 (1993).
[28] K. Nakashima, H. Hayashi, O. Shimizu, and S. Ishizuka, Neurosci. Res. (N.Y.) **40**, 325 (2001).
[29] R. E. Hampson, C. J. Heyser, and S. A. Deadwyler, Behav. Neurosci. **107**, 715 (1993).